JMEPEG (2005) 14:241-248
DOI: 10.1361/10599490523391

1059-9495/$19.00

Weldability and Microstructural Variations in Weldments of Ti-5Ta-1.8Nb Alloy

T. Karthikeyan, Arup Dasgupta, S. Saroja, and M. Vijayalakshmi

(Submitted October 8, 2003; in revised form July 23, 2004)

The successful replacement of the present generation of corrosion-resistant materials (nitric acid-grade stainless steel and Ti) by Ti-5Ta-1.8Nb, which has better corrosion resistance, depends on its weldability characteristics. This article presents the results of a study on the fabrication, qualification, and microstructural characterization of the welds. Welding was carried out using the direct current electrode negative (DCEN) polarity tungsten inert gas (TIG) (manual) welding method with high-purity Ar shielding. Testing was carried out as per the ASME standard (section IX, welding and brazing). Qualification tests found that the weldment met the required properties. The weldment showed heterogeneous microstructures, which are rationalized based on differences in phase transformation mechanisms that are dictated by the thermal cycles experienced by various microscopic regions. The results, described in this article, confirm that the weldability of the developmental Ti-Ta-Nb alloy is excellent. A preliminary evaluation of the corrosion behavior of the welds showed rates comparable to that of the base metal, establishing that this alloy could be considered as an alternative material for use in highly corrosive environments.

Keywords microstructure, solidification, titanium, Ti-5Ta-1.8Nb, weldment, weld qualification

1. Introduction

The electrolytic dissolver tank used for the dissolution of spent fuel in the fast reactor fuel reprocessing plant is exposed to aggressive chemical and radiation environments (Ref 1). The electro-oxidative dissolution process involves the dissolution of the spent fuel in boiling nitric acid. Therefore, the important considerations in the design of a dissolver tank are alloy structural integrity and long life to ensure safety and reduce the amount of high-level radioactive waste. These can be achieved by the careful selection of materials that possess excellent corrosion resistance along with good formability and welding characteristics. The latter is very important, because several metal joints, both similar (Ti-Ti) and dissimilar (Ti alloy-304L), are required in the construction of a reprocessing plant. Based on the evaluation of the corrosion properties of austenitic stainless steels, nuclear grade stainless steels, Ti, Zr, silicon-iron, and tantalum alloys at various concentrations and temperatures of nitric acid, Zr, and Ti (Ref 1, 2) were selected as suitable candidate materials for construction of the dissolver tank. In chemical plants employing nitric acid loops, Ti has proven to be the ideal material for pipes and other support structures. Additionally, the nature of corrosion in Ti is uniform compared with the localized type of corrosion (e.g., tunneling and intergranular) that occurs in stainless steels (Ref 3). Additionally, Ti is less prone to stress corrosion cracking in a nitric acid environment compared with Zr (Ref 4).

Pure unalloyed Ti exhibits good corrosion resistance (Ref 5). However, studies on the influence of various alloying elements, in concentrated nitric acid (Ref 6) have shown that the corrosion rates were further reduced with additions of Ta and Nb. The addition of up to 5 wt.% Ta reduced the corrosion rate by a factor of 7. It has also been reported (Ref 6) that the addition of 1 wt.% Nb reduced the corrosion rate by 13%. Hence, an alloy of nominal composition Ti-5Ta-1.8Nb is expected to offer the best corrosion resistance.

For ease of workability, the hot deformation of Ti alloys is generally carried out in the two-phase field of α (hexagonal close-packed [hcp]) + β (body-centered cubic [bcc]). The addition of Ta and Nb expands the $\alpha + \beta$ phase field, resulting in a larger temperature window for the hot working of the ingot. Hence, the Ti-Ta-Nb alloy is expected to be superior to Ti with respect to workability.

Besides corrosion resistance and formability, "acceptable weldability" is another important requirement if this alloy is to successfully replace the present generation of alloys. It is important that the weld structure (a) possesses adequate strength, (b) is devoid of embrittling phases, and (c) has corrosion properties comparable to the base metal (BM). Titanium is known to pick up O, N, C, H, and Fe at high temperatures (Ref 7), embrittling the structure even at low concentrations (i.e., at the level of parts per million). Thus, the welding of Ti and its alloys demands a high level of cleanliness to avoid impurity pickup. This is a crucial requirement in the construction of the dissolver tank. Additionally, the physical and mechanical properties of the BM, including thermal conductivity, thermal expansion, strength, and residual stress, and the welding process parameters, such as heat input, number of passes, and weld joint configuration, can influence the mechanical and corrosion properties of the weld joint.

The industrial performance of the weldment, especially with respect to corrosion behavior, is expected to depend on the

T. Karthikeyan, Arup Dasgupta, S. Saroja, and **M. Vijayalakshmi,** Materials Characterization Group, Indira Gandhi Centre for Atomic Research, Kalpakkam 603 102, India. Contact e-mail: mvl@igcar.ernet.in.

Table 1 Chemical composition of the Ti-Ta-Nb alloy

Element	Ta, wt.%	Nb, wt.%	Ti, wt.%	Impurities, (ppm) Fe	O	N	C	H
Content	4.39	1.94	Balance	263	501.5	47	125	9

microstructural heterogeneity of the weldment. One of the crucial parameters is the size of the β-grains in the weld (Ref 8). In addition, the difference in thermal exposure of various regions of the weldment results in a nonuniform distribution of β-grain size. Studies on wrought Ti-Ta-Nb alloy have shown that very coarse β grains form during exposure at temperatures in the β phase field. The grain sizes in the fusion zone (FZ) of the weldments of Ti alloys are an order of magnitude higher than that in the BM. Such rapid grain growth and nonuniform distribution of grain sizes markedly influence the properties of the weldment. In addition, welding imposes different cooling rates in different regions of the weldment. This, in turn, influences the microstructure and, hence, the mechanical properties. It is, therefore, essential to recognize the importance of the microstructure of the FZ and the heat-affected zone (HAZ) in determining the properties of a weldment. Hence, a systematic study of the microstructural features of the weldment of the Ti-Ta-Nb alloy has been carried out. The preliminary results on weldability characteristics and qualification of the weldment are presented in this article.

2. Experimental Details

The alloy, in the form of 12.5 mm ϕ cylindrical rods, and supplied by the Nuclear Fuel Complex (Hyderabad, India), was used for fabrication of the welds. The fabrication route for the alloy has been discussed elsewhere (Ref 9). The chemical composition of the alloy is given in Table 1. Due to the limited availability of the alloy, certain modifications were required prior to welding to carry out the weld qualification studies. The rods were rolled at room temperature into strips 300 × 15 × 3 mm in size. No intermediate stress relieving was done. The final rolled alloy was stress relieved by heating in a vacuum for 2 h at 923 K.

Six strips, 300 × 15 × 3 mm in size, were assembled to form a monolith structure (300 × 90 × 3 mm) by spot welding. These structures were then parted along the centerline to obtain two plates (150 × 90 × 3 mm). The plates were machined along the width to obtain a single-V groove. Welding was carried out by Titanium Tantalum Products Limited, Chennai, India. The welding and qualification tests were carried out as per the ASME standard (section IX, "Qualification Standards for Welding and Brazing Procedure") The qualification tests included visual examination, x-ray analysis, bend tests, and tensile tests on the weld joints.

The characterizations of the BM, FZ, and HAZ were carried out using optical and scanning electron microscopy (SEM). Specimens were prepared by standard metallographic methods. Specimens in the width-thickness (W-T) direction were macroetched using a reagent composed of 10 mL of HF + 25 mL of HNO_3 + 100 mL of H_2O, while a reagent composed of 3 mL of HF + 2 mL of HNO_3 + 95 mL of H_20 was used for microetching the samples. Transmission electron microscopy (TEM) was also performed on selected samples (Ref 10).

3. Results and Discussion

3.1 Characterization of the Base Metal

Figure 1(a) shows the SEM micrograph of the BM. The microstructure consists of recrystallized grains of α with a second phase dispersed as nodules. The Ti-5Ta-1.8Nb alloy has been classified as a two-phase α + β alloy based on its chemistry and room temperature microstructure (Ref 11). To identity the phases, analytical TEM was carried out on electron-transparent thin foils. The TEM micrograph is shown in Fig. 1(b). The presence of equiaxed grains with a second phase dispersed both along the grain boundaries and within the grains is clearly seen. The energy dispersive spectroscopy (EDS) spectra from the second phase and the matrix are shown in Fig. 1(c) and (d). The Ta and Nb content in the nodular particle is higher than that from the matrix. This suggests that the nodular phase is rich in Ta and Nb, and corresponds to β, while the solute depleted phase is the α matrix. This can be understood from the fact that both Nb and Ta are strong β stabilizers and have a tendency to repartition into the β phase. The structure of the BM consists of polygonal α with a uniform distribution of nodular β particles. This microstructure is in agreement with the structure expected in Ti alloys that has been subjected to thermomechanical processing followed by stress relieving (Ref 12).

3.2. Fabrication of Welds

The fusion welding processes that are most commonly used for Ti alloys are gas-tungsten arc, gas metal arc, plasma arc, laser, and electron beam. Though the vacuum environment provides better cleanliness in the case of electron beam welding, it has been observed that localized inert gas shielding can effectively protect a large weld zone (FZ). In addition to shielding, the cleanliness of the welded component is important in avoiding weld contamination. The gas-tungsten arc welding (GTAW) process offers a very efficient method for both the manual and automated application on an industrial scale for welding thin sections.

Thus, the manual GTAW welding process was used for the welding of 3 mm thick plates in the horizontal position (1G). The weld joints were prepared using filler wires, 1.6 mm ϕ, with a composition exactly the same as that of the BM. The welding geometry of the plate assembly is depicted in Fig. 2. The plate edges were machined to obtain a V-groove subtending a total angle of 70 degrees, and the root gap width was kept at 2 mm. Welding was carried out in a clean room with continuous purging using Ar gas for the shielding, trailing, and backing actions during welding. Using the direct current electrode negative (DCEN) polarity with a thorium oxide added tungsten (thoriated W) welding torch, the weld joint was produced in a single pass on the face side followed by a root pass. The details of the process and process parameters are listed in Table 2. A high-energy density was selected to achieve full penetration during the single pass rather than employing a multipass weld procedure. This experimental approach was expected to minimize distortions and residual stresses.

The metal flowed from the filler rod to the weld pool (WP) smoothly, and the weld joint was successfully obtained using the stringer bead technique. Visual inspection of the weldment revealed a uniform surface, free from gross surface defects. There was no discoloration of the surface. In addition, the weldment exhibited a bright luster finish, signifying little or no

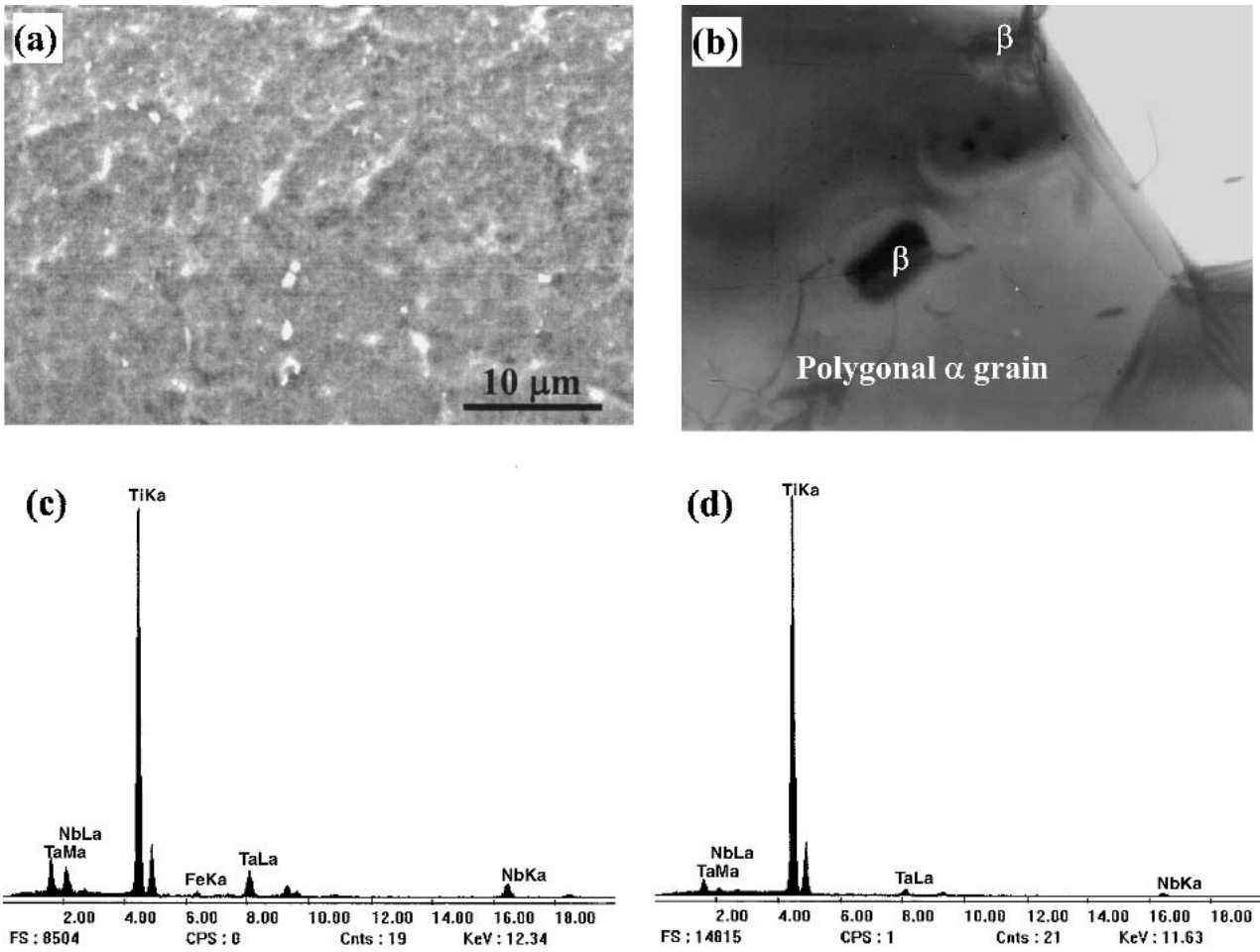

Fig. 1 (a) SEM image of the BM showing equiaxed α and β nodules; (b) TEM micrograph showing the presence of β nodules along prior β boundaries and within the equiaxed α phase; (c) EDS spectra from the β particle; and (d) EDS spectra from the α matrix. Higher amounts of Ta and Nb are seen in the β phase relative to the α phase.

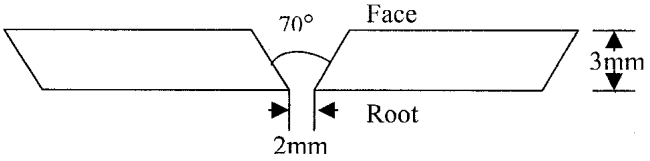

Fig. 2 Geometry of the W-T section of weldment

impurity pickup during welding. Visual inspection showed that the Ti-Ta-Nb plates could be welded easily by the manual GTAW process. Having established a welding process, the quality of the welds was evaluated.

3.3 Qualification of the Ti-Ta-Nb Welds

The ASME standard (section IX) prescribes the tests for procedure qualification. The tests include nondestructive x-ray analysis to evaluate the presence of subsurface defects in the weld joint. Mechanical tests, namely, tensile and guided bend tests (in both face-bend and root-bend configurations) on a ground flat surface, were performed to evaluate the joint strength. Tests were repeated for reproducibility.

Radiography showed no evidence of porosity, thus qualifying the joint to be free from internal porosity defects. The weld joint passed the complete 180 degree bend test without any cracking in both the face-bend and root-bend configurations. Figure 3 shows a photograph of the tested specimens. Dye penetrant further confirmed the U-bend specimens to be free from surface cracks.

Table 2 Welding procedure and parameters

Welding process	Manual GTAW
Type of joint	V-groove, both side welded, single pass per side
Material specification	
1. Base metal	3 mm thick Ti-5Ta1.8N plate
2. Filler metal	1.6 mm ϕ Ti-5Ta1.8Nb wire
Postweld heat treatment	None
Gas	
1. Shielding gas	Ar (99.995% pure) @ 6 L/min
2. Trailing gas	Ar (99.995% pure) @ 35 L/min
3. Backing gas	Ar (99.995% pure) @ 35 L/min
Welding characteristics	DCEN
1. Amps	50–80
2. Volts	12–14
3. Tungsten electrode size	ϕ 3.0 mm
4. Travel speed	60–80 mm/min
5. No. of passes	2

Note: DCEN, direct current electrode negative

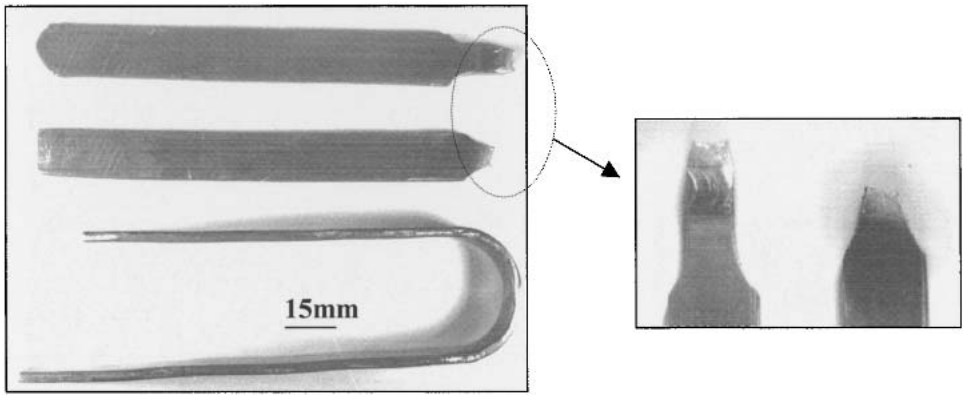

Fig. 3 Photograph of tensile and guided bend test specimens. Fracture outside the weld joint is clearly visible.

An examination of the tensile tested specimen showed necking prior to fracture, suggesting ductile failure. A closer examination of the fracture surface showed that failure occurred outside the FZ (Fig. 3). The SEM fractograph of the tensile-tested specimen is shown in Fig. 4, clearly showing the classic ductile failure characteristics. The measured values for ultimate tensile strength from the tensile tests of the two specimens were 530 and 525 MPa. These test results showed that the weld joint possesses adequate strength. Although these values were lower than those reported (Ref 9) for the BM, the strength of the weld joint was satisfactory for use as a dissolver tank material. Based on these studies, the procedure qualification record (PQR) of the weld and the welding procedure specification (WPS) for the Ti-5Ta-1.8Nb alloy have been established. Preliminary tests for the corrosion behavior of the weld joint in boiling 11.5 M nitric acid showed that the corrosion rate was comparable to that of the BM (~0.3 mpy). The detailed evaluation of the liquid, vapor, and condensate corrosion rates of the weldment is in progress.

The microstructural variations within the weldment and the extent to which they vary from that of the BM are strongly influenced by the temperature experienced by different regions of the weldment. A detailed characterization of the weld and HAZ microstructures as a function of distance from the heat source is underway to determine the possible thermal cycles experienced by different regions of the weldment.

3.4 Microstructural Variations in the Weldment

Earlier studies on the wrought Ti-Ta-Nb alloy have shown that the decomposition of the high-temperature bcc β phase into the α + β phase is sensitive to the rate of cooling, resulting in a wide range of microstructures (Ref 12-14). Each of these structures possesses characteristic morphology, crystal structure, and microchemistry features, depending on the nature on the coexisting phases. These are, in turn, dictated by the temperature and cooling rate. A systematic study on the transformation behavior of the β phase has been performed (Ref 10, 13). As such, an understanding of the microstructures that would result when the alloy is subjected to different temperatures and cooling rates has provided the basis for analyzing the weld microstructures. However, caution has to be exercised when extending microstructure or property evaluation of the isothermally heat-treated wrought alloy to the weldment. Weldments are subjected to continuous cooling at different rates at different locations.

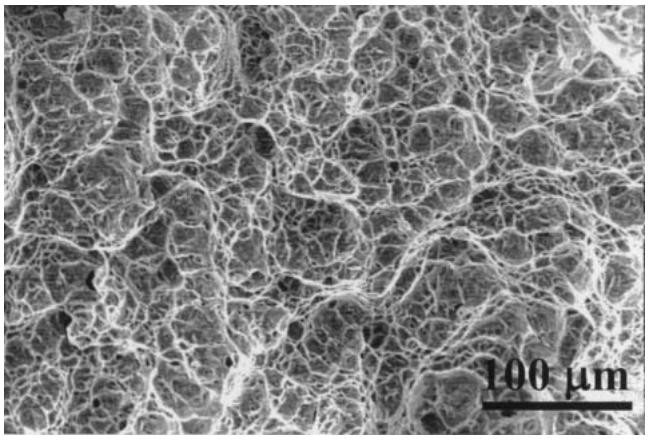

Fig. 4 SEM fractograph showing the ductile nature of the fracture in the tensile tested specimen

Continuous cooling during weld solidification is expected to result in the formation of nonequilibrium phase transformation products in the alloy. As a preliminary step, the microstructures that form in different regions of the weld joint as a function of distance from the heat source have been identified and compared with the microstructures that form during isothermal heat treatments.

3.4.1 Characterization of the Weld Region The macroscopic W-T sectional view of the FZ of the weld joint is shown in Fig. 5. A similar solidification pattern and structure is seen on both the face and root sides. However, the structure formed during the subsequent root pass is more prominent. The specks of black in the micrograph were diagnosed at high magnification to be etch pits, and the FZ was actually found to be porosity free. Various subzones within the FZ were observed, and the transition boundaries resemble the constant temperature profile expected during the butt weld joining of plates. The GTAW process adopted for fusion welding of the Ti-Ta-Nb plates involved an intense heat source leading to the meltback of the BM. Because the filler rods were from the same heat as the BM and no flux was used, the dilution effects are expected to be low. Additionally, the use of Ar gas for backing, trailing, and shielding minimizes impurity pickup. The thinness of the plates (3 mm), and the use of a single pass on the face and root sides, were expected to minimize the residual stresses.

It is well known that the heat flow and fluid flow in the WP exert a significant influence on the temperature gradients in the

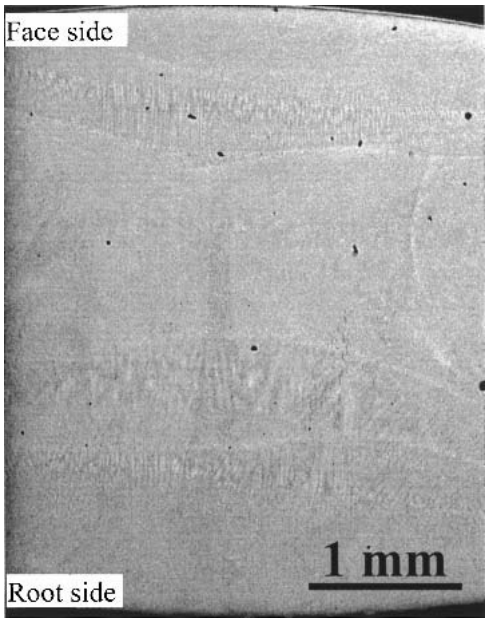

Fig. 5 SEM micrograph of the weld showing the face and the subsequent root-pass

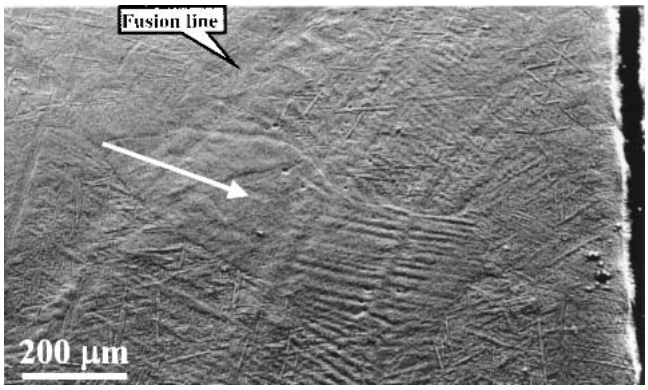

Fig. 6 SEM image of the weld in the macro-etched condition showing evidence of epitaxial solidification. The growth of the grains in the BM close to the fusion line into the weld is clearly seen.

WP, and, hence, on solidification behavior. An SEM micrograph of the weld region of the Ti-Ta-Nb alloy is shown in Fig. 6. Significant grain growth has occurred in the BM, from which the grains of the weld metal have grown. Such grain growth is expected in the BM closest to the fusion line (i.e., the region corresponding to the boundary between melted and unmelted metal), which experiences the highest temperature. This suggests that the initial process of solidification is epitaxial. This is in agreement with information from the literature (Ref 15) on fusion welding, in which the initial solidification is mostly observed to be epitaxial and the partly melted grains of the BM at the fusion boundary act as nucleation sites for new grain growth.

It was seen that the direction of crystal growth during solidification was not random. The optical micrograph of the weld region in the macroetched condition is shown in Fig. 7(a). A columnar structure is clearly observed with grain lengths approximately 2 mm in length. The formation of such coarse grains during solidification has been reported in several Ti alloys (Ref 8). The observed variation in the width of the columnar grain is attributed to the combined effects of the solidification processes during the face and root passes, and to the reheating of the weld during the root pass. The direction of growth was observed to be normal to the fusion boundary. This can be understood, because the direction of the growth of columnar grains is always along the direction of the steepest temperature gradients in the weld. It has been reported that the crystals tend to grow along certain preferred crystallographic directions (i.e., <100> for most cubic materials), because this is one of the loosely packed directions in the crystal (Ref 15) and allows a faster growth velocity than those achieved in other directions.

A uniformly lamellar structure was observed within the columnar grains. This structure has been identified as transformed β phase, consisting of alternate lamellae of the α + β phase. This compares well with the structures obtained by the $\beta \rightarrow \alpha + \beta$ phase transformation during isothermal treatments in the β phase field. The formation of a transformed β phase by Widmanstatten transformation of the high-temperature β phase has been established in earlier studies (Ref 13, 14).

From Fig. 7(a), it can be seen that each individual grain exhibits a substructure. Regions very close to the face and root pass show a substructure within the columnar grain. The macrostructure of the FZ toward the face pass is shown in Fig. 7(b). In region A, a grain consisting of an array of cells separated from each other by low-angle boundaries is observed. The substructure on the top shows the presence of an array of irregular cubes. The direction of growth is expected to be parallel to the welding direction, suggesting that the temperature gradient was highest along that direction. Cellular microstructures are reported (Ref 16) to be stable only for a certain range of temperature gradients. They become unstable, and develop secondary and tertiary arms that develop into a dendritic structure as the temperature gradient decreases. Thus, the observed structure on the top surface of the weld is a cellular-dendritic-type in which the formation of secondary and tertiary arms is suppressed due to the relatively small temperature gradient. Cell spacing in this region is on the order of 10 μm. Such a fine size is attributed to the high-cooling rates at the surface.

The structure of region B is shown in Fig. 7(b). A structure consisting of a parallel array of dendrites is observed that is similar to that found in region A. The dendrite arm spacing is 15 μm, which is higher than that in region A. This is attributed to the relatively lower temperature gradients in this region and is in agreement with the reported formation of dendrites at the centerline of welds where the temperature gradient is lowest (Ref 15). This also corresponds to the region of the weld where the growth rate is at its maximum compared with the welding speed (Ref 17). The direction of grain growth is normal to the heat source, and this also corresponds to the direction of maximum heat flow. The change in direction of growth between regions A and B is expected from the general solidification behavior observed in most metals (Ref 16). Similar structures were obtained on the root side, confirming that the solidification behavior was identical on the face and the root sides. A detailed investigation on the solidification behavior and solute repartitioning is in progress.

3.4.2 Microstructural Heterogeneities in the Heat-Affected Zone For ease of understanding the microstructural variations, the HAZ has been divided into five zones, which is shown schematically in Fig. 8. The initial microstructure of the HAZ is the same as that of the BM, which is equiaxed α with

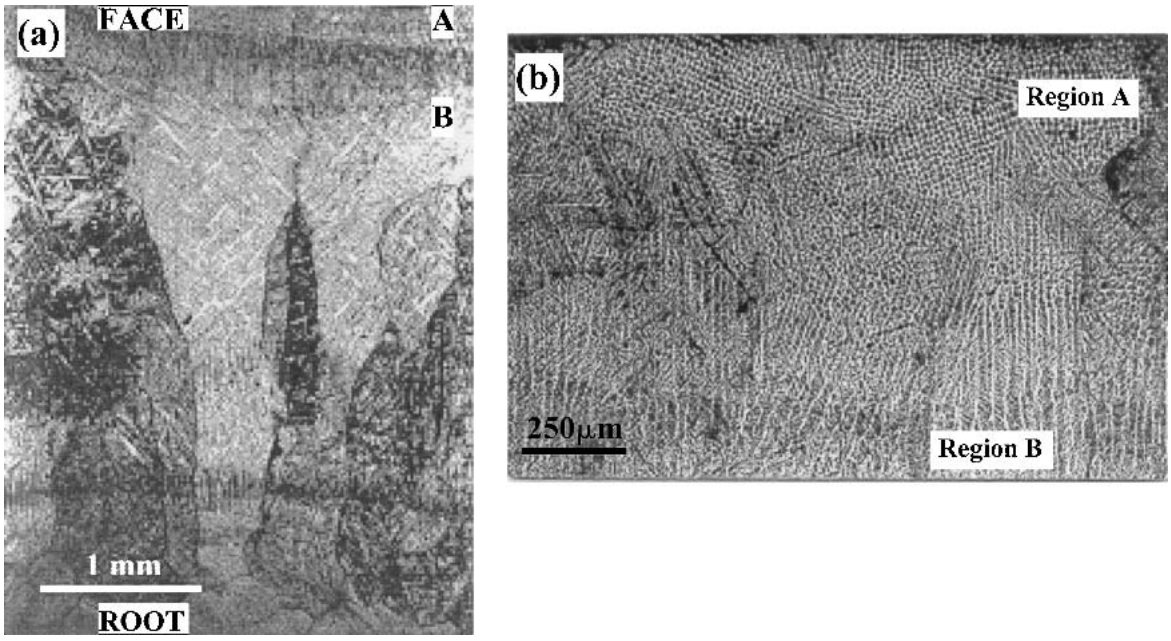

Fig. 7 (a) Optical micrograph of the weld region in the macro-etched condition showing the growth of columnar grains. The cellular-dendritic structures near the face and root surfaces are also seen. (b) A magnified view of the cellular-dendritic structures on the face side. Region A is close to the surface, and region B is beneath region A.

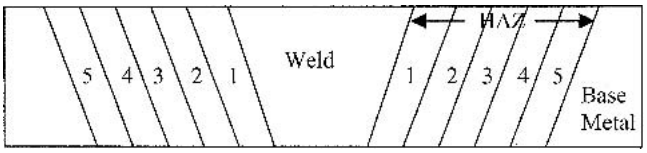

Fig. 8 Schematic of the W-T section of the weldment. The HAZ is divided into regions 1 to 5 to study the variation of microstructures as a function of distance from the fusion line.

β nodules. The other microstructures obtained in the HAZ are described below.

The microstructure of region 1, which is very close to the fusion boundary, is shown in Fig. 9(a). Very coarse β grains (100 μm) are observed. This is attributed to the temperature excursion in this region, which is highest for the solid that did not melt. The complete dissolution of all the preexisting phases and the consequent increased mobility of the solutes at this temperature would result in uninhibited grain growth of the β grains. The large grain size is also due to the low (95 kJ/mol) activation energy for grain growth of bcc Ti (Ref 18). A fully transformed β structure consisting of acicular α is observed within the grains. This is in agreement with the structure observed in the wrought alloy, where the β phase transforms into α + β phases via a Widmanstatten mechanism, resulting in a transformed β structure (Ref 10, 13). The uniform formation of the transformed β phase suggests that this region has entered into a fully β phase field, and the large-grain size suggests that it has experienced temperatures far exceeding the β transus of the alloy. The grain size was, however, lower than that obtained for the wrought alloy (~250 μm) when subjected to an isothermal heat treatment for 2 h at 1273 K (Ref 13). This corresponds to the short time spent at high temperature in the case of welding. The acicular α phase is fine with no evidence of grain boundary α. This is attributed to the high-temperature gradient and fast-cooling rate found in this region. Studies on the influence of cooling rate on the transformation mode of the β phase have suggested that grain boundary α does not form for cooling rates greater than 0.03 K/s. The transformation of the BM in this region can be summarized as:

$$\text{Equiaxed } \alpha + \beta \text{ nodules} \rightarrow \beta \rightarrow \text{acicular } (\alpha + \beta)$$

The adjacent region, labeled as 2 (Fig. 9b), shows large β grains (40 μm) with α grains along the boundaries and a uniformly transformed β grain within. The uniform structure and β grain size suggest that the temperature was sufficiently above the β transus but lower than the temperature in region 1. The presence of grain boundary α suggests that the cooling rate in this region was slow compared with region 1. The lower cooling rate also favored the Widmanstatten transformation of the high-temperature β phase. The transformation can be summarized as:

$$\text{Equiaxed } \alpha + \beta \text{ nodules} \rightarrow \beta \rightarrow \text{acicular } (\alpha + \beta) + \text{grain boundary } \alpha$$

Region 3 (SEM micrograph in back-scattered mode, Fig. 9c) showed a significantly different structure from regions 1 and 2. The presence of small amounts of primary α grains (arrow) along the triple points, and grain boundaries of the prior β grains, coexisting with large regions of transformed β grains, was observed. The confirmation of primary α grains was obtained based on lower amounts of Ta and Nb in the plate-like α grains. In addition, the number density of β nodules was reduced compared with the BM though a few nodules of β grains remained. The retention of β grains was attributed to the high amounts of Ta and Nb (confirmed by EDS), which tend to stabilize the structure. The solute concentration was distinctly different between the retained β grains and the primary α grains. The bright particles in Fig. 9(c) possess very

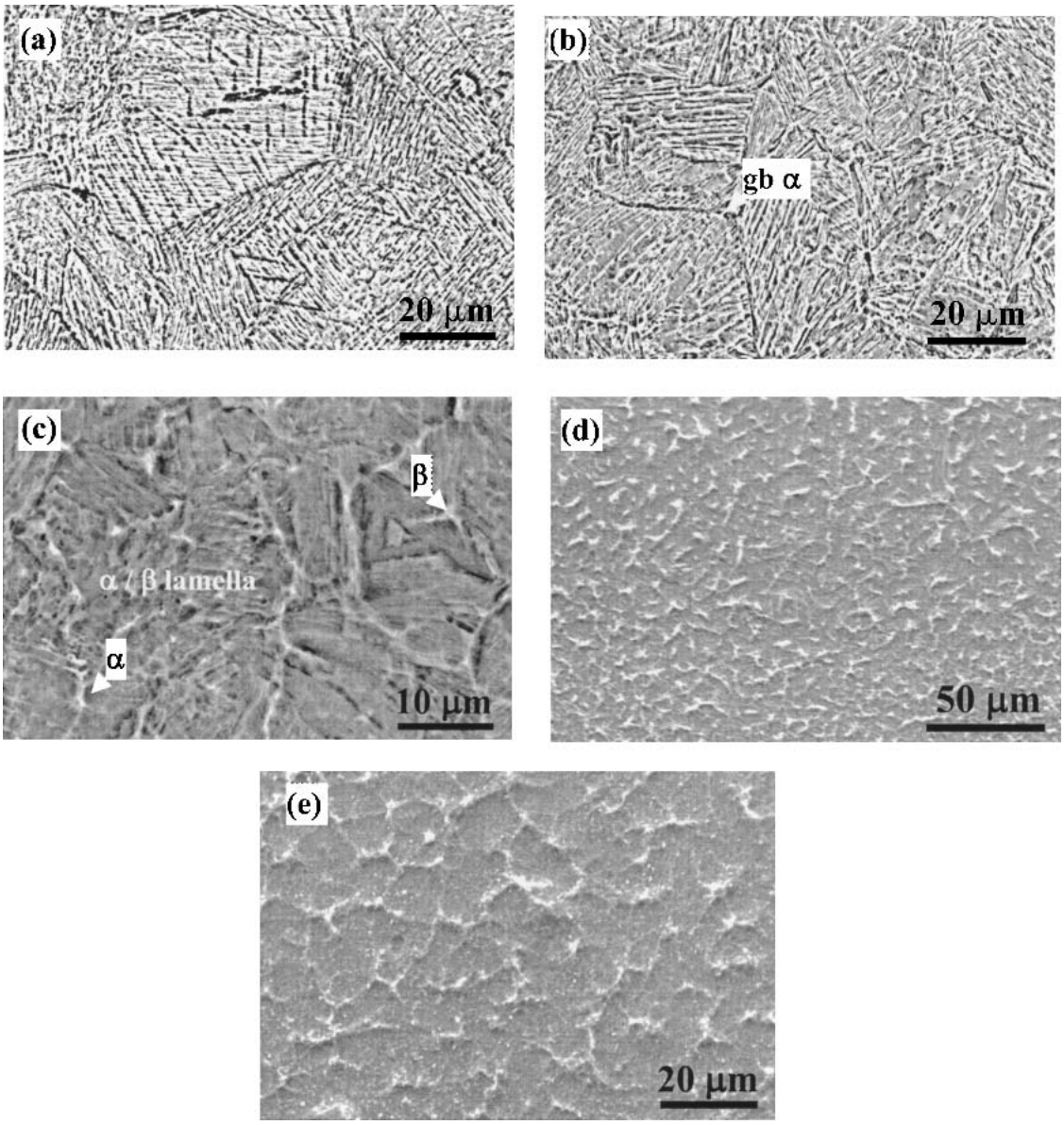

Fig. 9 SEM micrographs in the HAZ of the Ti-5Ta-1.8Nb weldment showing the variation in microstructure with distance from the fusion line. (a) Region 1 showing coarse grains with fully transformed β nodules. (b) Region 2 showing transformed β nodules and the grain boundary (gb) of α. (c) Region 3 showing transformed β nodules (α/β lamella) coexisting with primary α and retained β nodules. (d) Region 4 showing the growth of β nodules. (e) Region 5 close to the BM showing the coalescence of α nodules.

high amounts of Ta and Nb, which is characteristic of the β phase, while the primary α grains were solute lean. The absence of a transformation substructure also confirmed that these regions corresponded to the α phase. The short duration of the high temperature was possibly inadequate for the β phase to become homogeneous. Hence, the highly enriched β phase in the BM was partly retained, while the β nodules that were nucleated and grown at the high temperature underwent the Widman-statten transformation during cooling, resulting in the lamellar product. The small-grain size (~10–15 μm) was attributed to (1) the lower temperatures and (2) the presence of the second phase. This suggests that this region experienced temperatures below the β transus, resulting in the presence of primary α plates. The volume fraction of the α phase was less than that in the BM. The low amounts of α phase suggest that this temperature was in the upper portion of the α + β phase field. The transformation is summarized as follows:

Equiaxed α+ β nodules → primary α + β → Acicular (α + β) + primary α + β nodules

The microstructure of region 4 is shown in Fig. 9(d). The structure predominantly consisted of α phase, along with small amounts of β phase. The size and amount of the β phase is higher than that in the BM. This microstructure suggests that region 4 experienced a lower temperature in the α + β phase field compared with that in region 3. The observed growth of the β phase compared with that of the BM can be understood in terms of the higher amount of β phase expected at temperatures higher than the stress-relieving treatment given to the BM.

Region 5 shows the growth and coalescence of the equiaxed α grains. The β nodules observed in the BM are also observed. This suggests that the temperature experienced in this region is low in the α + β phase field where the growth of β would be

very slow. During the short exposure time, no observable change in the amount of β was expected. The transformation in regions 4 and 5 can be summarized in the following way:

Equiaxed α+ β nodules → α + β → Equiaxed α + β

The microstructural characterization shows that the microstructures in the HAZ show a systematic variation with distance from the fusion boundary. The microstructures change from a very coarse grain-transformed β structure near the fusion line to an equiaxed α + β structure toward the BM. This variation can be understood in terms of the transformation characteristics of each phase, which are dictated in large part by the maximum temperature experienced in each region of the BM during the welding cycle.

3.5 In Summary

- Welds were fabricated by a manual GTAW process using Ar gas for shielding, trailing, and backing.
- Visual inspection, x-ray analysis, and 180 degree U-bend and tensile tests showed that the weld joints were free of defects and embrittling phases.
- Tensile tests showed that the weld joint had adequate mechanical strength for the intended application. Fracture was ductile and occurred outside the weld.
- Characterization of the weld showed that the initial solidification in the weld was epitaxial.
- The microstructures in the HAZ showed systematic variation with distance from the fusion line, and these structures were dictated by the maximum temperature experienced by each region.

4. Summary and Conclusion

The weldment of the alloy Ti-5Ta-1.8Nb has been fabricated using a manual GTAW process. The test welding and weld qualification tests were performed as per the ASME standards (section IX). The weld joint passed the qualification tests satisfactorily. Based on the studies, the PQR of the test weld and the WPS have been formulated. The structures in the weldment have been understood in terms of the possible solidification and phase transformation mechanisms.

Acknowledgment

The authors thank Dr. V.S. Raghunathan, Associate Director, MCG and Dr. Baldev Raj, Director, Indira Gandhi Centre for Atomic Research, for initiating this project, and for their keen interest and support throughout the course of this work.

References

1. B. Raj, U.K. Mudali, T. Jayakumar, K.V. Kasiviswanathan, and R. Natarajan, *Sadhana,* Vol 26 (No. 6), 2000, p 519-559
2. U.K. Mudali, R.K. Dayal, and J.B. Gnanamoorthy, *J. Mater. Eng. Perform.,* Vol 4, 1995, p 756-760
3. U.K. Mudali, R.K. Dayal, and J.B. Gnanamoorthy, *J. Nucl. Mater.,* Vol 203, 1993, p 73-82
4. H. Nagano, H. Kajimura, and K. Yamanaka, *Mater. Sci. Eng. A,* Vol A198, 1995, p 127-134
5. J.D. Destefani, Introduction to Titanium and Titanium Alloys, *Metals Handbook,* Vol 2, 10th ed., ASM International, 1990, p 586-591
6. A. Takamura, K. Arakawa, and Y. Moriguchi, Corrosion Resistance of Titanium and Titanium-5% Tantalum Alloy in Hot Concentrated Nitric Acid, *Proc. Int. Conf. on Science, Technology and Applications of Titanium,* R.I. Jaffee and N.E. Promisel, Ed., Pergamon Press, 1970, p 209-216
7. W.A. Baeslack, D.W. Becker, and F.H. Froes, *J. Metals,* Vol 36, 1984, p 46-58
8. S. Sundaresan, G.D. Janaki Ram, and G. Madhusudhan Reddy, *Mater. Sci. Eng. A,* Vol 262, 1999, p 88-100
9. K. Kapoor, V. Kain, T. Gopalkrishna, T. Sanyal, and P.K. De, *J. Nucl. Mater.,* Vol 322, 2003, p 36-44
10. R. Mythili, V. Thomas Paul, S. Saroja, M. Vijayalakshmi, and V.S. Raghunathan, Study of Transformation Behavior in a Ti-4.4Ta-1.9Nb Alloy, *J. Mater. Sci. Eng. A*, Vol 390, 2005, p 299-312
11. R. Mythili, S. Saroja, M. Vijayalakshmi, and V.S. Raghunathan, Determination of Processing Window for Hot Working of Ti-5wt%Ta-1.8wt%Nb Alloy for Reprocessing Applications, *Proc. Conf. on Mater. and Technol. for Nucl. Fuel Cycle,* B. Raj, K.B.S. Rao, P. Shankar, and N. Murali, Ed., Board of Research in Nuclear Sciences, Indian Nuclear Society, and Indian Institute of Metals, 2003, p C29-C34
12. R. Mythili, S. Saroja, M. Vijayalakshmi, and V.S. Raghunathan, Design of Heat Treatments for Optimum Microstructure in Ti-5wt%Ta-2wt%Nb Alloy, *Proc. Conf. on Mater. and Technol. for Nucl. Fuel Cycle,* B. Raj, K.B.S. Rao, P. Shankar, and N. Murali, Ed., Board of Research in Nuclear Sciences, Indian Nuclear Society, and Indian Institute of Metals, 2003, p C24-C28
13. T. Karthikeyan, A. Dasgupta, S. Saroja, and M. Vijayalakshmi, Texture Development during β → α Transformation in Severely Cold Rolled Ti-Ta-Nb Alloys Treated Above β Transus, I.D. Garg, Ed., *Proc. XXVI Annual Conf. on Elec. Microscy. and Allied Fields,* EMSI, 2003, p 197-198
14. T. Karthikeyan, Arup Dasgupta, S. Saroja, M. Vijayalakshmi, A.J. Khan, D. Bhattacharjee, and V.S. Raghunathan, *Commun. Mater. Sci. Eng. A.,* Vol A393, 2005, p 294-302
15. K. Easterling, *Introduction to The Physical Metallurgy of Welding,* 2nd ed., Butterworth-Heinemann Ltd., Oxford, UK, 1992.
16. O. Grong, *Metallurgical Modelling of Welding,* 2nd ed., The Institute of Materials, London, UK, 1997
17. M. Rappaz, S.A. David, J.M. Vitek, and L.A. Boatner, *Metall. Trans.,* Vol 20A, 1989, p 1125-1138
18. F.J. Gil, M.P. Genebra, J.M. Manero, and J.A. Planell, *J. Alloys Compd.,* Vol 329, 2001, p 142-152